European Congress on Computational Methods in Applied Sciences and Engineering
ECCOMAS 2004
P. Neittaanmäki, T. Rossi, S. Korotov, E. Oñate, J. Périaux, and D. Knörzer (eds.)
Jyväskylä, 24–28 July 2004

AN EXTENDED FINITE ELEMENT STRATEGY FOR THE ANALYSIS OF CRACK GROWTH IN DAMAGING CONCRETE STRUCTURES

Claudia Comi[⋆], **Stefano Mariani**[‡] **and Umberto Perego**[⋄]

Dipartimento di Ingegneria Strutturale, Politecnico di Milano
Piazza L. da Vinci 32, 20133 - Milano (Italy)

e-mail: [⋆]claudia.comi@polimi.it, [‡]stefano.mariani@polimi.it, [⋄]umberto.perego@polimi.it

web page: http://www.stru.polimi.it/Ccosmm/ccosmm.htm

Key words: quasi-brittle materials, non-local damage, cohesive models, extended finite element method.

Abstract. *An integrated strategy is proposed for the simulation of damage development and crack propagation in concrete structures. In the initial stage of damage growth, the concrete is considered to be macroscopically integer and is modeled by a non-symmetric isotropic nonlocal damage model. The transition to the discrete cohesive crack model depends on the local mesh size and is driven by an analytical estimate of the current bandwidth. When a crack is introduced in the model an extended finite element strategy is used to follow the propagation without modification of the background mesh. The proposed methodology is tested on a notched tension specimen and then applied to the analysis of a concrete gravity dam.*

1 INTRODUCTION

Existing large concrete dams often exhibit visible cracks which may be caused by several circumstances, such as: alcali-aggregate reaction or other reactions with chemicals contained in the basin water, pressurized water infiltrations, thermal effects either due to the concrete maturing process or seasonal oscillations [1, 2, 3]. On the other hand, exceptional loading conditions like, e.g., earthquakes, overtopping waves produced by sudden floods, landslides or ground motions beneath the dam, may induce catastrophic propagation of pre-existing cracks or may lead to the growth of damage in the concrete body of the dam, with final nucleation of new cracks.

The current state-of-the-art in finite element technology envisages two approaches for structural simulation of fracture processes: a continuum approach, where fracture is seen as the end of a process of localization and accumulation of damage in a continuum, without creating a real discontinuity in the material (see e.g. [4, 5, 6]); a discrete approach, where a displacement discontinuity with an interface endowed with a cohesive constitutive behaviour is artificially introduced in the model at a loading level, in a direction, with a length and at a position which have to be determined according to physically motivated criteria [7, 8, 9, 10].

Continuum approaches are based on the definition of a material model with softening post-peak behaviour and therefore require a regularization to avoid pathological mesh dependence. Among several alternatives, the nonlocal continuum approach can effectively reproduce the damage process and its localization within a mesh-independent band, provided that the element size is small enough to resolve the band (at least three constant strain elements within the band). Therefore, for a given mesh it is in principle possible to define the minimum bandwidth which can be resolved with that mesh. When, due to the development of damage, the bandwidth reduces below this threshold, the finite element simulation becomes unreliable unless the mesh is refined. However, for real structures as large concrete dams, the computational cost becomes soon unacceptable. Furthermore, the discontinuous approach based on a cohesive crack model, which is certainly more convenient from a computational point of view, is unable to describe the first phase of diffused structural damage. The alternative approach here followed consists of carrying out first a continuum damage analysis until the bandwidth becomes smaller than the critical value associated to the used mesh and then, only at that point, of introducing a discrete cohesive crack [11, 12]. An estimate of the localization bandwidth and conditions for the transition from the continuum damage analysis to a damage analysis with a propagating displacement discontinuity are proposed on the basis of an energy conservation criterion. Numerical tests, including an application to a benchmark exercise recently proposed by ICOLD, show the promising performances of the proposed methodology.

2 PROBLEM FORMULATION

2.1 Bulk constitutive model

The material behavior of the bulk is described by a nonlocal isotropic damage model.

The model is based on the simplifying assumption, reasonable for quasi-brittle materials under stress states of prevailing tension, that the only dissipation mechanism be tension damage. The model can be enhanced by adding a compression damage mechanism as proposed e.g. in [6]. The local format of the constitutive relations reads:

$$\sigma = (1-D)\,\mathbf{E} : \varepsilon \tag{1}$$

$$f = 2\mu^2 \mathbf{e} : \mathbf{e} - 9K^2 a\, \varepsilon_v^2 + 3Kb \ln^{\frac{n}{2}} \left(\frac{c}{1-D} \right) \varepsilon_v - k \ln^n \left(\frac{c}{1-D} \right) \leq 0 \tag{2}$$

$$\dot{D} \geq 0, \qquad f\dot{D} = 0 \tag{3}$$

where σ is the stress tensor, ε is the small strain tensor, $\mathbf{E}$ is the elasticity tensor, D is the isotropic damage variable, μ and K are the elastic shear and bulk moduli of the virgin material, $\mathbf{e}$ is the deviator of ε, ε_v is the volumetric strain, a, b, c, k and n are material parameters defining the initial elastic domain $f = 0$ and its evolution. The meridian section of the loading function f in the stress space is a hyperbola, with vertex on the hydrostatic axis for $b^2 > 4ak$ and asintotes inclined of $\sqrt{a}$. Figure 1 shows the initial loading function in the plane stress case for different values of coefficient a. The evolution with damage of the elastic domain is governed by parameters c and n and follows the same law proposed in [13]. Assuming continuous loading, the inelastic stress-strain relation under uniaxial conditions can be obtained in closed form and reads

$$\sigma = c \exp \left[- \left(\frac{b + \sqrt{b^2 + 4\left(\frac{1}{3} - a\right) k}}{2k} E\varepsilon \right)^{\frac{2}{n}} \right] E\varepsilon \qquad \text{for } \varepsilon \geq \varepsilon_0 \tag{4}$$

where E is the Young modulus and ε_0 is the linear elastic limit strain. The corresponding stress-strain curves are shown in Figure 2 for different values of parameter n.

Nonlocality is introduced in the model by replacing in the loading function f the strain invariants $\mathbf{e} : \mathbf{e}$ and ε_v by their weighted averages, denoted by a superposed bar, defined as follows

$$\overline{\mathbf{e} : \mathbf{e}}\,(\mathbf{x}) = \int_\Omega W(\mathbf{x}, \mathbf{s})\, \mathbf{e}(\mathbf{s}) : \mathbf{e}(\mathbf{s})\, d\mathbf{s}, \qquad \bar{\varepsilon}_v(\mathbf{x}) = \int_\Omega W(\mathbf{x}, \mathbf{s})\, \varepsilon_v(\mathbf{s})\, d\mathbf{s} \tag{5}$$

$$W(\mathbf{x}, \mathbf{s}) = \frac{1}{\bar{W}(\mathbf{x})} \exp \left(-\frac{\|\mathbf{x} - \mathbf{s}\|^2}{2l^2} \right), \; \bar{W}(\mathbf{x}) = \int_\Omega \exp \left(-\frac{\|\mathbf{x} - \mathbf{s}\|^2}{2l^2} \right) d\mathbf{s} \tag{6}$$

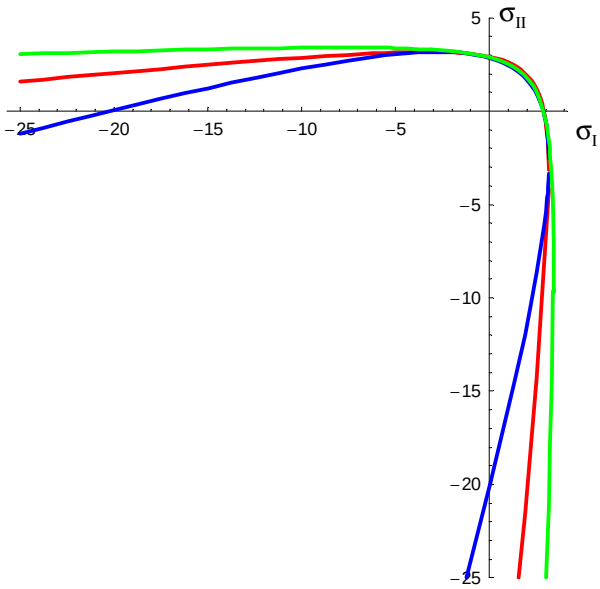

Figure 1: Loading function for different values of a.

where $W(\mathbf{x}, \mathbf{s})$ is the weight function, here assumed as the Gauss function, normalized to be able to reproduce a constant field accounting for the effect of the boundary on the interaction. In (6) l is a geometric parameter related to the width of the process zone, in the terms which will be discussed in the next Section.

The nonlocal version of the model described above has the advantage that, despite the nonlocality of the model, all constitutive calculations can be carried out locally at each Gauss point separately ([14] and [15]). Other choices are also possible with different physical and computational implications (see e.g. [16] for a review).

2.2 Critical damage and band direction

An effective indicator of the current bandwidth can be obtained studying the conditions for the propagation of a harmonic stress wave of wave number q in a uniformly strained bar of infinite length, with a nonlocal material behavior, as presented in [17]. The conditions under which the wave can propagate along the bar, i.e. the conditions ensuring a real phase velocity, are sought. The wave propagation analysis follows exactly the same path explained in [17] and even though the model here considered is nonsymmetric in tension and compression, the final estimate of the bandwidth turns out to be the same. The critical value of q, or equivalently the critical wave length $\lambda_{cr} = \frac{2\pi}{q_{cr}}$ such that only waves with wavelength $\lambda < \lambda_{cr}$ do propagate results

$$\lambda_{cr} = \sqrt{2}\pi l \left[-\ln\left(\frac{n}{2} \ln^{-1} \frac{c}{1-D} \right) \right]^{-0.5} \tag{7}$$

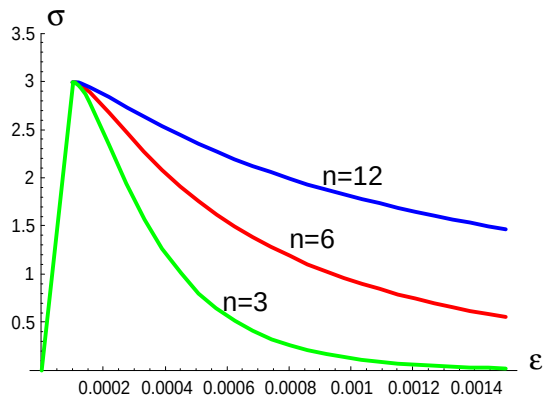

Figure 2: Uniaxial stress-strain curves.

Waves with $\lambda > \lambda_{cr}$ cannot propagate and the strain field remains uniform. Therefore, the width of the localization band is directly related to the maximum wavelength λ_{cr}. According to equation (7), this internal length is a positive, decreasing function of damage tending to zero as damage tends to one, as shown in Figure 3.

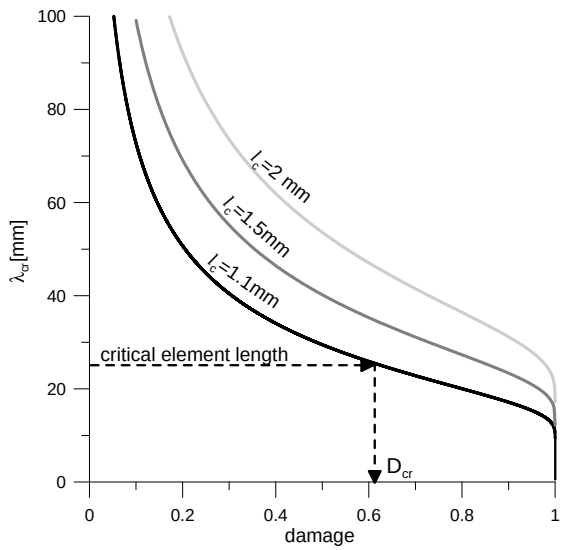

Figure 3: Evolution of the bandwidth with damage.

Even though the hypotheses under which the expression (7) has been derived are very restrictive (one dimensional problem, bar of infinite length, homogeneous initial state) it provides a rough but useful estimate of the bandwidth, which can be used to assess the usability of the current mesh in relation to the current value of damage. Defining by s_e

the typical size of the finite element in the localization zone, the minimum bandwidth which can be resolved is given by $L_e = n_e s_e$ (with n_e=3-5, meaning that at least 3-5 elements are needed across the localization band). Imposing that the critical wavelength (i.e. the bandwidth) be bigger then L_e, i.e.

$$\lambda_{cr} \geq n_e s_e = L_e \tag{8}$$

and solving (7) for D, one can define a critical damage value

$$D_{cr} = 1 - c \exp\left[-\frac{n}{2} \exp\left(\frac{2\pi^2 l^2}{L_e^2}\right)\right] \tag{9}$$

Figure 3 shows schematically the definition of D_{cr}. This value turns out to depend on the chosen mesh, through L_e, it tends to one as the element size tends to zero and it also depends on the material internal length l of the non-local model. D_{cr} is assumed as the damage value at which the transition has to be triggered: when in an element one has $D > D_{cr}$, a crack is introduced in that element according to the methodology illustrated in Section 3.

The initial direction of the crack can be assigned on the basis of the damage field accumulated in the continuum until that moment, requiring the crack to have the same direction of the already formed damage band.

2.3 Cohesive law

A second important issue concerning the transition from the continuum to the discrete approaches to fracture is the definition of the properties of the cohesive crack originating from the continuum model at the moment of the transition. Restricting for simplicity to mode I propagation, the constitutive behaviour of a cohesive crack is defined by a relation between the normal component t of cohesive traction and the normal component w of displacement discontinuity across the crack.

The strategy here proposed is to define the t vs w law in such a way that, at the moment of the transition, the residual energy which would be dissipated within the damage localization band in the continuum approach (denoted by C), with a very fine mesh, is the same which can be dissipated by a discrete crack introduced at that stage within the band (approach denoted by C-D). Consider first the C-approach and a localization band of width $\lambda_{cr}(\varepsilon)$ with a local coordinate m in its cross direction. The total energy which can be dissipated in the band is

$$G_C = \int_0^{\infty} \int_{-\frac{\lambda_{cr}(\varepsilon)}{2}}^{\frac{\lambda_{cr}(\varepsilon)}{2}} \sigma \, dm \, d\varepsilon \tag{10}$$

Consider now the C-D approach. Since the crack is introduced for $D = D_{cr}$, corresponding to $\varepsilon = \varepsilon_c$, the work density produced by the continuum problem up to this point is

$$G_1 = \int_0^{\varepsilon_c} \int_{-\frac{\lambda_{cr}(\varepsilon)}{2}}^{\frac{\lambda_{cr}(\varepsilon)}{2}} \sigma \, dm \, d\varepsilon \tag{11}$$

and the corresponding bandwidth is

$$\lambda_{cr}\left(\varepsilon_c\right) = L_e \tag{12}$$

When the discontinuity is introduced, the material in the surrounding band unloads and the elastic energy recovered upon complete unloading is given by

$$G_2 = L_e \frac{1}{2} E\left(1 - D_{cr}\right)\varepsilon_c^2$$

To make the C-approach and the C-D-approach energetically equivalent, the crack model should be endowed with a fracture energy

$$G_3 = G_C - \left(G_1 - G_2\right)$$

This can be obtained, e.g., by the following definition of the t vs w law under loading conditions

$$\begin{aligned} t\left(w\right) =& c \exp\left[-\left(\frac{b + \sqrt{b^2 + 4\left(\frac{1}{3} - a\right)k}}{2k} E(\varepsilon_c + w/L_e)\right)^{\frac{2}{n}}\right] E(\varepsilon_c + w/L) \\ &+ \frac{1}{2} E\left(1 - D_{cr}\right)\varepsilon_c^2 \frac{w}{L_e} \exp\left[-\frac{w}{L_e}\right] \end{aligned} \tag{13}$$

Note that the above analysis holds for mode I only. The procedure can however be generalized to more complex fracture processes.

3 FINITE ELEMENT IMPLEMENTATION

Let us consider the domain Ω: a mesh of constant strain triangles with nodes (belonging to set I) placed only at element vertices is adopted for the entire C-D analysis, i.e for the continuous nonlocal damage analysis and for the subsequent cohesive crack propagation analysis. When, according to the proposed transition criterion, a crack Γ_d has to be introduced in the finite element model, an extended finite element strategy (Belytschko and co-workers [18, 19]) is followed in the form developed in [10] for cohesive crack propagation.

Let $\phi_i\left(\mathbf{x}\right)$, $i \in I$, $\mathbf{x}$ being the position vector, be the usual piecewise linear nodal shape functions. Discontinuous displacement fields across Γ_d can be modelled by enriching the interpolation field as follows:

$$\mathbf{u}^h\left(\mathbf{x}\right) = \sum_{i \in I} \phi_i\left(\mathbf{x}\right)\mathbf{u}_i^0 + \sum_{j \in J}\sum_{h} H\left(\mathbf{x}\right)\phi_j\left(\mathbf{x}\right)\psi_{hj}\left(\mathbf{x}\right)\mathbf{u}_{hj}^E \tag{14}$$

where the set J collects those nodes whose support is cut by Γ_d. $H(\mathbf{x})$ is the generalized Heaviside step-function, defined as:

$$H(\mathbf{x}) = \begin{cases} +1 & \text{if} \quad (\mathbf{x}-\mathbf{x}^*)^T \mathbf{m} > 0 \\ -1 & \text{if} \quad (\mathbf{x}-\mathbf{x}^*)^T \mathbf{m} < 0 \end{cases} \tag{15}$$

$\mathbf{x}^*$ being the closest point projection of $\mathbf{x}$ onto Γ_d. The enrichment functions $\psi_{hj}(\mathbf{x})$ are assumed to be polynomial functions (up to order $h-1$) of the position vector $\mathbf{x}$. In the specific applications considered in this paper $h=1$, hence ψ_{hj} are constant functions. In Equation (14), $\mathbf{u}_i^0$ are the basic nodal degrees of freedom, while $\mathbf{u}_{hj}^E$ are the enhanced ones.

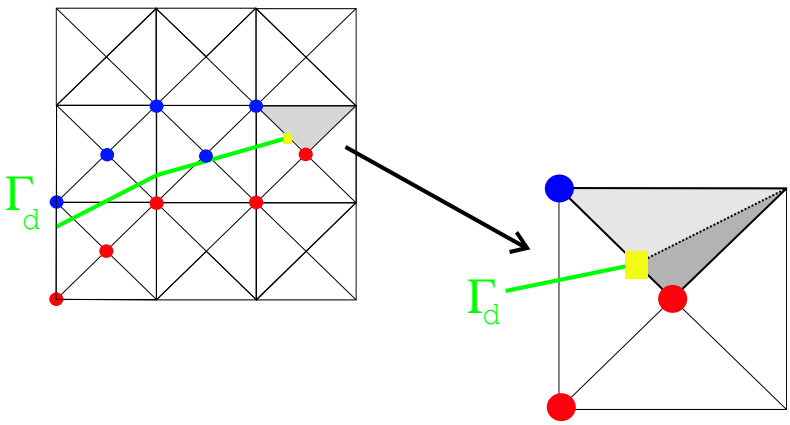

Figure 4: Sketch of the cohesive-tip region.

During crack propagation, the element ahead the current crack-tip, marked by a yellow square in Figure 4, is modified to avoid spurious locking response in the tip region. It is necessary that the kinematics of this element allows a stress free (rigid body) opening of the crack thus allowing for unloading of the material in the elements crossed by the crack and loading of the cohesive process zone. The kinematic modification of the tip element is based on a sub-triangularization, as shown in Figure 4. In the sub-elements, only the two nodes shared by the adjacent element containing the crack tip are enhanced (nodes marked with circles in the right close-up in the figure). In this way, a continuous displacement field is obtained ahead of the crack tip while strain discontinuity is allowed. Besides avoiding mesh locking, this method allows to unambiguously identify the regions where $H(\mathbf{x}) = +1$ (with blu nodes in Figure 4) and where $H(\mathbf{x}) = -1$ (with red nodes in Figure 4).

4 NUMERICAL RESULTS

4.1 Tension test on a double-edge-notched specimen

The first example concerns the simulation of a direct tension test on a double-edge notched specimen (DENT test). The two-dimensional geometry shown in Figure 5 has been considered. A non-structured mesh of plane strain finite elements has been adopted with a characteristic element dimension $s_e = 2$ mm, see Figure 5. According to the proposed continuous-discontinuous strategy, several analyses have been carried out assuming different values of n_e, namely $n_e = 3, 5, 7$, in the transition criterion, Eq. (8).

The global responses of the specimen in terms of vertical reaction versus imposed vertical displacement for different n_e (continuous curves) are compared in Figure 6 with the results obtained with a continuum approach, without crack propagation (dotted curve). Thanks to the energy equivalence imposed for the transition, good agreement is obtained. Since the mesh used for this problem is very fine compared to the material internal length, when $n_e = 3$ is chosen, transition occurs very late in the analysis and the same response of the continuum approach is obtained.

The distribution of the tension damage variable D and the crack evolution for the different analyses (constant element size s_e and varying minimum number n_e of elements required across the band) is shown in Figure 7 at four increasing values of imposed displacement. Damage starts to grow at the notch and then develops in a horizontal band. When damage reaches the critical value given by Eq. (9), a cohesive crack is introduced; this crack propagates in the ligament until complete failure of the specimen. As expected when n_e increases, transition to a cohesive crack model is anticipated and final damage values in the cracked band are smaller.
Figure 8 shows, at an enlarged scale, the pattern of damage evolution and crack propagation for $n_e = 5$. It can be noted that the transition to a cohesive crack and the subsequent propagation occur in the region and in the direction of the highest damage localization. The direction of propagation is not affected by the layout of the background mesh.

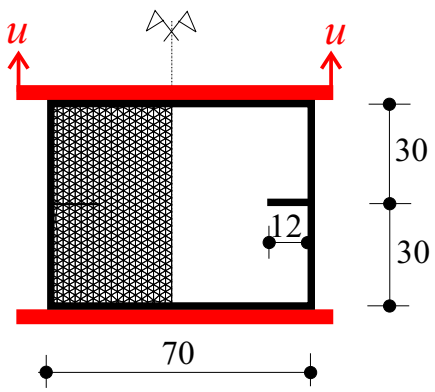

Figure 5: Geometry of the double-notched specimen (measures in mm).

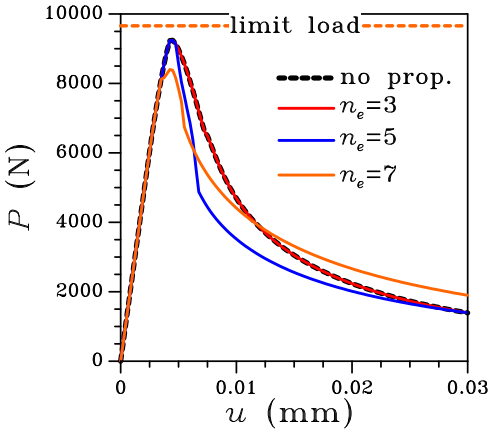

Figure 6: DENT test. Effect of n_e on the load vs imposed displacement plot at fixed $s_e = 2$ (mm).

4.2 Failure analysis of a concrete gravity dam

The proposed methodology has been applied to the benchmark exercise A2 proposed by ICOLD in 1999 [20]. The benchmark consists of the evaluation of the IFF (Imminent Failure Flood) as a consequence of an overtopping wave acting on a concrete gravity dam whose geometry is specified in Figure 9. The dam lays on a rock bed.

The loading condition analysed consists of the constant dam self-weight and of the hydrostatic pressure due to a water level in the reservoir growing from zero to the overtopping level (which can be higher than the dam) which causes the failure of the dam. A portion of the rock foundation has also been included in the mesh.

The material data for concrete and rock used for the identification of the model parameters are those assigned in [20]; an internal length $l = 250$ mm has been assumed, corresponding to about 2 times the maximum aggregate size expected to be present in a dam. The analysis has been performed using both the continuous approach up to failure and the continuous-discontinuous approach. The results are shown in Figure 10 in terms of the overtopping coefficient (defined as water level divided by dam height) versus horizontal crest displacement. Structural failure corresponds to lack of convergence in the performed load-controlled analyses. The same failure prediction is obtained by the two approaches. Figure 11a shows the damage pattern at failure obtained by the nonlocal damage model in the region at the dam foot enclosed in the square in Figure 9b. Figure 11b refers to the analysis with crack propagation: similar damage patterns are obtained in the two analyses because of the fine mesh adopted and the ensuing high value of critical damage governing the transition.

Acknowledgments.
This work has been carried out with the financial support of MIUR-PRIN 2002087915-2002 contract.

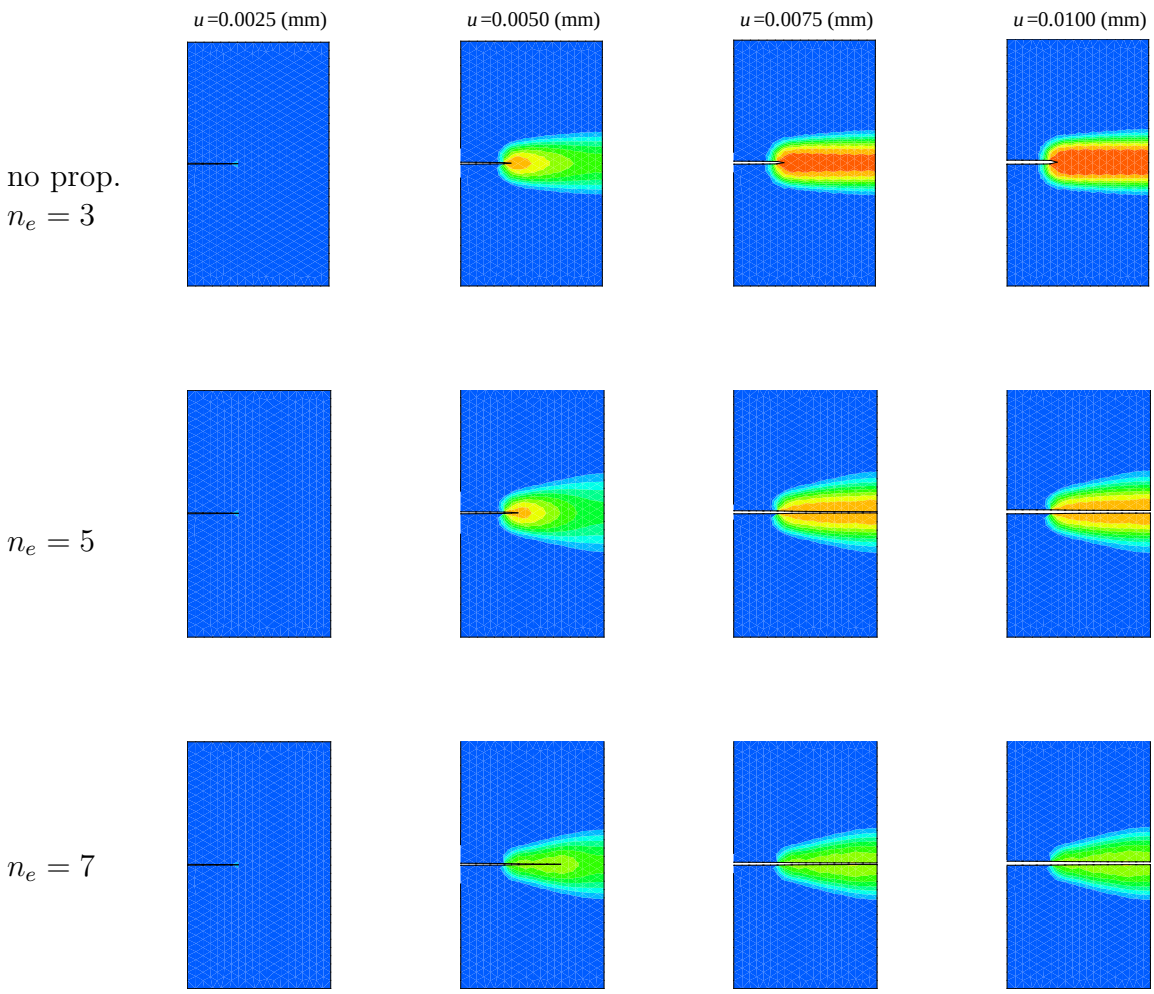

Figure 7: DENT test. Effect of n_e ($s_e = 2$ mm) on damage pattern and crack evolution up to $u = 0.01$ (mm).

REFERENCES

[1] V. E. Saouma, E. Bruhweiler, and H.L. Boggs. A review of fracture mechanics applied to concrete dams. *International Journal of Dam Engineering*, 1:41–57, 1990.

[2] P. Léger, P. Côté, and R. Tinawi. Finite element analysis of concrete swelling due to alkali-aggregate reactions in dams. *Computers and Structures*, 60:601–611, 1996.

[3] B. Capra and A. Sellier. Orthotropic modeling of alkali-aggregate reaction in concrete structures: numerical simulations. *Mechanics of Materials*, 35:817–830, 2003.

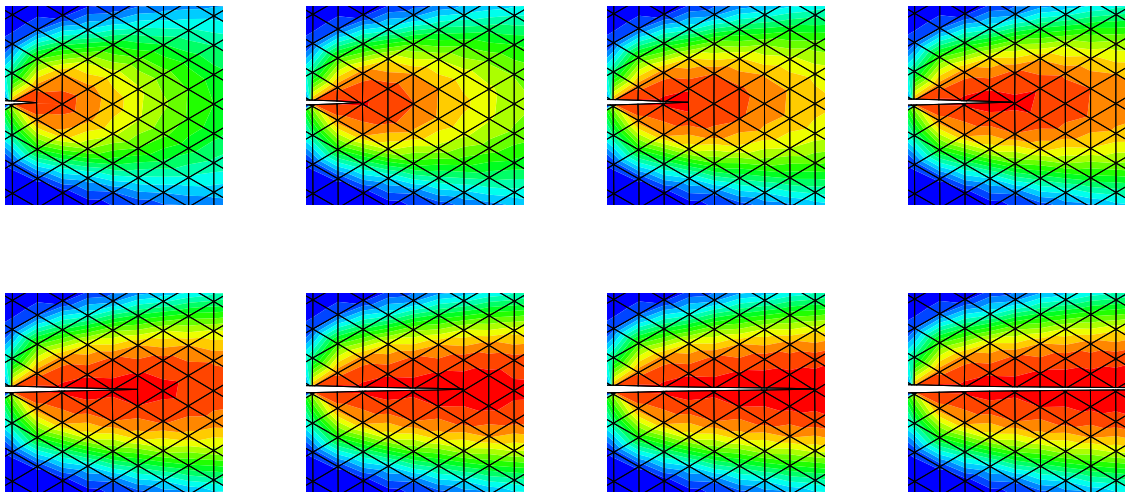

Figure 8: DENT test, $s_e = 2$ (mm), $n_e = 5$. Close-up of the ligament region with details of damage evolution and propagating cohesive crack.

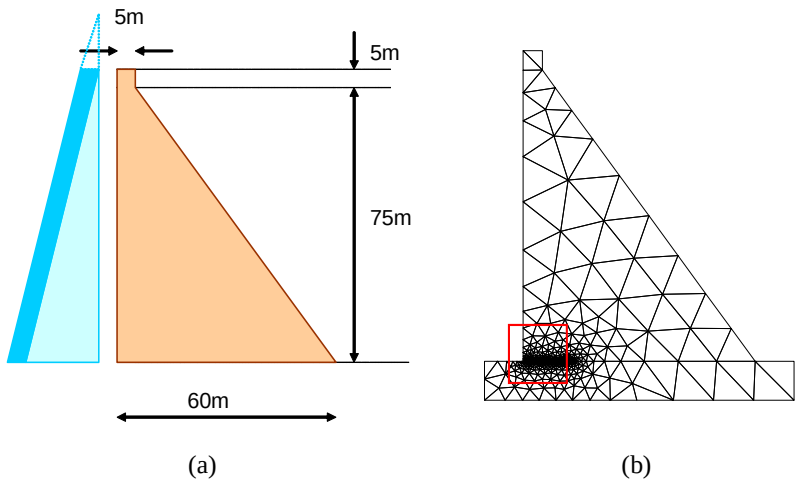

Figure 9: ICOLD Benchmark. a) problem geometry, b) adopted mesh.

[4] M. Cervera, J. Oliver, and R. Faria. Seismic evaluation of concrete dams via continuum damage models. *Earthquake Engineering & Structural Dynamics*, 24:1225–1245, 1995.

[5] R.H.J. Peerlings, R. de Borst, W.A.M. Brekelmans, and M.G.D. Geers. Gradient-enhanced damage modelling of concrete fracture. *Mechanics of Cohesive-Frictional*

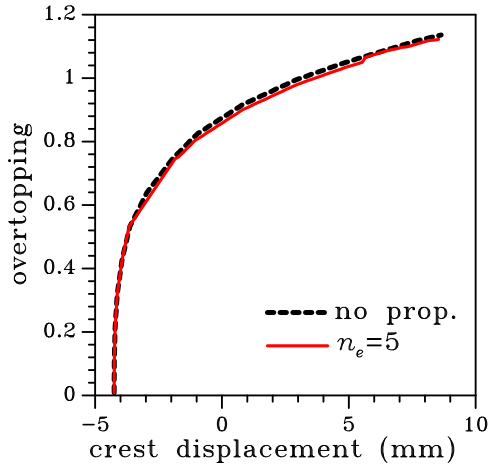

Figure 10: ICOLD Benchmark. Effect of the propagating cohesive crack on the horizontal crest displacement vs overtopping coefficient plot.

Materials, 3:323–342, 1998.

[6] C. Comi and U. Perego. Fracture energy based bi-dissipative damage model for concrete. *International Journal of Solids and Structures*, 38:6427–6454, 2001.

[7] P. Bocca, A. Carpinteri, and S. Valente. Mixed mode fracture of concrete. *International Journal of Solids and Structures*, 27:1139–1153, 1991.

[8] X.-P. Xu and A. Needleman. Numerical simulation of fast crack growth in brittle solids. *Journal of the Mechanics and Physics of Solids*, 42:1397–1434, 1994.

[9] M. Jirasek. Comparative study on finite elements with embedded cracks. *Computer Methods in Applied Mechanics and Engineering*, 188:307–330, 2000.

[10] S. Mariani and U. Perego. Extended finite element method for quasi-brittle fracture. *International Journal for Numerical Methods in Engineering*, 58:103–126, 2003.

[11] C. Comi, S. Mariani, and U. Perego. On the transition from continuum nonlocal damage to quasi-brittle discrete crack models. In *Proceedings of the Third Joint Conference of Italian Group of Computational Mechanics and Ibero-Latin American Association of Computational Methods in Engineering*, 2002.

[12] C. Comi, S. Mariani, and U. Perego. From localized damage to discrete cohesive crack propagation in nonlocal continua. In H.A. Mang, F.G. Rammerstorfer, and J. Eberhardsteiner, editors, *Proceedings of the Fifth World Congress on Computational Mechanics (WCCM V)*. Vienna University of Technology, 2002.

[13] C. Comi and U. Perego. Numerical aspects of nonlocal damage analyses of concrete structures. *Revue Europeenne des Elements Finis*, 10:227–242, 2001.

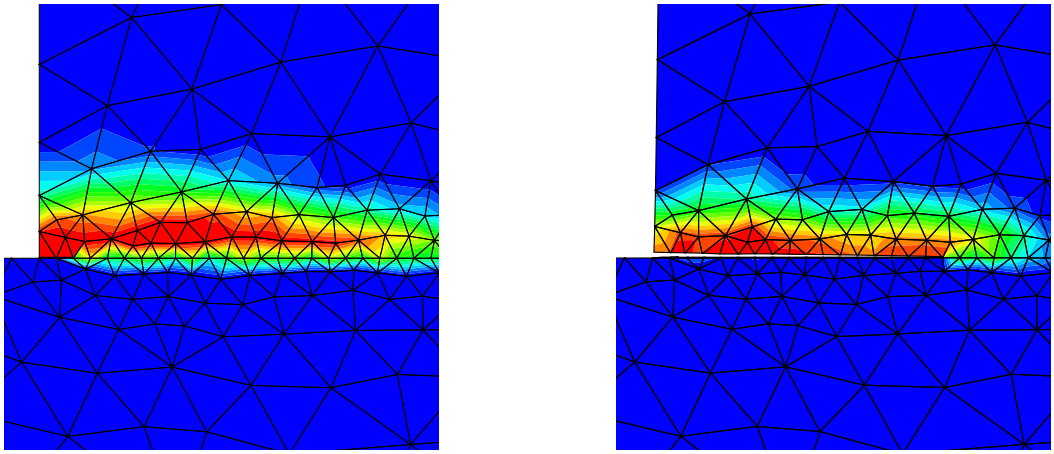

(a) (b)

Figure 11: ICOLD Benchmark. Close up at the dam-foundation interface showing the damage pattern at collapse (a) with the continuum approach and (b) allowing for cohesive crack growth.

[14] G. Pijaudier-Cabot and Z. L. Bažant. Nonlocal damage theory. *ASCE, Journal of Engineering Mechanics*, 113:1512–1533, 1987.

[15] C. Comi. A non-local model with tension and compression damage mechanisms. *European Journal of Mechanics A/Solids*, 20:1–22, 2001.

[16] M. Jirasek. Nonlocal models for damage and fracture: Comparison of approaches. *International Journal of Solids and Structures*, 35:4133–4145, 1998.

[17] C. Comi and U. Perego. Symmetric and non-symmetric non-local damage formulations: an assessment of merits. In *Proceedings of ECCM-2001, European Conference on Computational Mechanics*, Cracow (Poland), June 2001.

[18] N. Moës, J. Dolbow, and T. Belytschko. A finite element method for crack growth without remeshing. *International Journal for Numerical Methods in Engineering*, 46:131–150, 1999.

[19] N. Moës and T. Belytschko. Extended finite element method for cohesive crack growth. *Engineering Fracture Mechanics*, 69:813–833, 2002.

[20] *Fifth International Benchmark Workshop on Numerical Analysis of dams, Theme A2*. ICOLD, Denver, Colorado, 1999.